Journal of Sound and Vibration (2002) **250**(3), 431–444
doi:10.1006/jsvi.2001.3952, available online at http://www.idealibrary.com on IDEAL®

HIGH-FREQUENCY RADIATION OF L-SHAPED PLATES BY A LOCAL ENERGY FLOW APPROACH

V. Cotoni, A. Le Bot and L. Jezequel

Laboratoire de Tribologie et Dynamique des Systèmes, École Centrale de Lyon, 36, *Avenue Guy de Collongues* 69131, *Écully*, *BP*163, *France*.
E-mail: *cotoni@mecasola.ec-lyon.fr*

(*Received* 1 *November* 2000, *and in final form* 26 *June* 2001)

This paper describes a local energy approach to predict the high-frequency radiation of structures. This general approach is applied to a two-dimensional problem of the radiation of two joined semi-infinite, baffled plates, below their critical frequency. The first step consists in determining how energy travels through subsystems and, for this purpose, elementary waves are studied. Then some canonical problems are solved to describe the behaviour of waves impinging on boundaries. Below the critical frequency, flexural waves are subsonic and their radiation is due to diffraction phenomena. According to the locality principle, the corresponding canonical solutions are used in the whole system resolution; power sources are introduced on boundaries to account for energy exchanges and, with the assumption that waves are uncorrelated, the energy contributions of all sources are simply summed.

1. INTRODUCTION

Several research papers have extensively studied the radiation of structures into acoustic media and it is still an important problem for industries. For high frequencies in the audio band, specific approaches based on energy quantities, such as SEA [1] or, more recently, local energy flow methods [2, 3] have been developed. The latter lead to more precise results than SEA as they give the spatial distribution of energy inside subsystems. On the other hand, energy flow methods need a more accurate description of systems as well as more CPU time. They have been already applied to the problem of radiation of plates inside a cavity [4, 5]. This paper presents the development of such a coupling for the radiation of plates in exterior acoustical media, which corresponds to a problem where the acoustical field is not diffuse.

The structural and acoustical systems are described according to an integral energy approach [3, 6]. The first step of the method is to study elementary waves and to calculate energy fields attached to these waves. Some boundary sources are introduced in order to check the local power balance on couplings between subsystems. Energy fields inside subsystems then result from the superposition of all source contributions.

A comparison may be drawn with the Geometrical Theory of Diffraction [7]. Firstly, in both methods, solutions are sought in terms of elementary travelling waves. For homogeneous media, these waves are plane, cylindrical and spherical, also thought of in terms of rays in the Geometrical Theory of Diffraction. Secondly, by virtue of the locality principle valid at high frequency [7, 8], a complex problem is divided into rather more simple canonical problems involving the vicinity of the interaction process. From each canonical problem, resulting boundary sources are introduced and evaluated. A simple

0022-460X/02/080431 + 14 $35.00/0

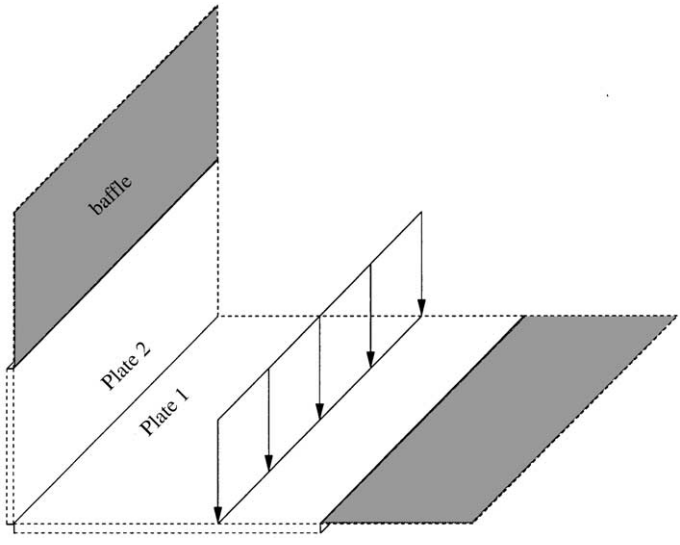

Figure 1. Two baffled, right-angled, semi-infinite structures, one of them being line excited.

summation of all source contributions is then achieved according to the locality principle. Finally, both methods extend the classical geometrical acoustics since they account for diffraction phenomena.

The main difference between the Geometrical Theory of Diffraction and the energy flow approach is that the latter deals directly with energy quantities. Indeed, the elementary waves are thought of in terms of energy, without any phase, and canonical problems are considered in terms of power balance. For this reason, the summation of the contributions of all power sources is performed assuming that waves are uncorrelated, thus considering that energy quantities are additive. Another difference is that radiation problems involve the diffraction of flexural waves into the acoustical medium leading to a wave conversion phenomenon. These phenomena are not encountered in the Geometrical Theory of Diffraction usually applied to acoustics or electromagnetics where only one medium is involved.

This paper focusses on the radiation of two baffled right-angled plates loaded by a fluid on the internal side. The plates are semi-infinite and one of them is line excited, reducing the problem to a two-dimensional case (see Figure 1). However, three-dimensional calculations have already been performed and compared with experimental results in reference [9]. The frequency range below the critical frequency of the fluid-loaded plates is investigated and consequently structural waves are subsonic.

The decomposition of the complete energy fields into elementary waves is carried out in the next section. The several canonical problems encountered in the system are then described in section 3. In section 4, the governing energy equations are derived in order to solve the system. Finally, a numerical comparison between energy results and a reference calculation is presented in the last section.

2. DECOMPOSITION OF ENERGY FIELDS

Vibration fields of systems at high frequency are assumed to be composed of uncorrelated elementary waves. The first step of the energy formulation is to characterize how energy carried by these waves propagates through systems.

2.1. DESCRIPTION OF THE ENERGY PROPAGATION

Due to the two-dimensional geometry, structures are thought of as one-dimensional systems and the acoustical medium as a two-dimensional system. Since the systems are homogeneous, the elementary waves involved in the description of vibration fields are plane and cylindrical waves. The energy density G_i and the intensity vector $\mathbf{H}_i$, corresponding to direct fields of sources are derived below. The subscript $i = 1, 2, a$ refers to the kind of wave. $i = 1$ for flexural waves in plate 1, $i = 2$ for flexural waves in plate 2 and $i = a$ for acoustical waves. The well-known local power balance applied to an infinitesimal volume under the harmonic dependence with pulsation ω, is written as [3]

$$\operatorname{div} \mathbf{H}_i + \eta_i \omega G_i = \delta(S), \tag{1}$$

where η_i is the damping loss factor assumed to be light ($\eta_i \ll 1$). The right-hand side is a unit power being injected in the volume at point S. Let c_i denote the group speed of waves in system i and $\mathbf{u}$ the unit vector in the propagation direction. The property of the elementary waves,

$$\mathbf{H}_i = c_i G_i \mathbf{u}, \tag{2}$$

which states that energy propagates with the group speed c_i towards $\mathbf{u}$, gives G_i and $\mathbf{H}_i$ as solutions of equation (1) in terms of the source point S and the receiving point M [3],

$$G_i(S, M) = \frac{1}{c_i} \frac{\mathrm{e}^{-\eta_i \omega r / c_i}}{\gamma_0 r^{n-1}}, \qquad H_i(S, M) = \frac{\mathrm{e}^{-\eta_i \omega r / c_i}}{\gamma_0 r^{n-1}} \mathbf{u}_{SM}, \tag{3}$$

where $r = [SM]$ and $\mathbf{u}_{SM}$ is the unit vector in the direction from S to M. $n = 1$, $\gamma_0 = 2$ for $i = 1, 2$ (flexural plane waves), and $n = 2$, $\gamma_0 = 2\pi$ for $i = a$ (acoustical cylindrical waves). These solutions are energy and intensity variations for plane or cylindrical waves generated by a power source with a uniform directivity and a unit magnitude in an infinite damped medium. They are now introduced in the energy flow formulation to achieve the energy description of systems.

2.2. DESCRIPTION OF THE COMPLETE SYSTEM

With the hypothesis that elementary waves are uncorrelated, energy quantities at any point of the system are the sum of the contributions of several power sources. These sources are determined now for both structures and the acoustical medium. For the sake of simplicity, it is assumed that structures may be seen as rigid for acoustical waves. This means that the acoustical power transmitted to the structures is neglected, which corresponds to a light fluid hypothesis.

For structures, two kinds of sources are introduced [3]. The first one is the primary source located on S and whose magnitude is ρ_s due to the excitation on plate 1. It produces the structural direct field. The others are located on the boundaries A, B and C of structures and describe the reverberant fields due to reflection and transmission effects. Two boundary sources are thus introduced for each structure. Their respective magnitudes are denoted as σ_A^1, σ_B^1 for plate 1 and σ_B^2 and σ_C^2 for plate 2. These structural sources are presented in Figure 2.

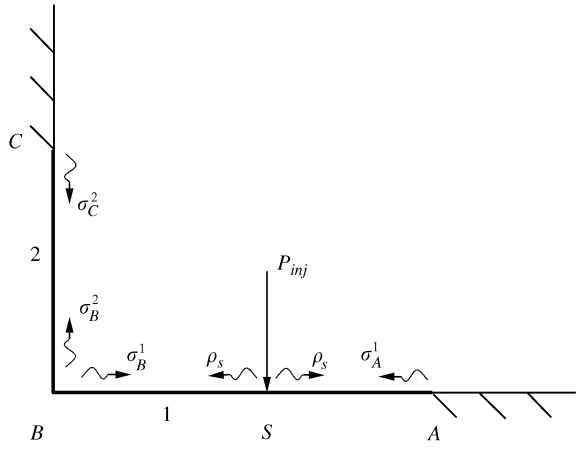

Figure 2. Two baffled, right-angled structures, with the structure 1 being line excited on the point *S*. Five structural power sources, σ_C^2, σ_B^2, σ_B^1, ρ_s, σ_A^1 are used to describe structures.

The following forms are obtained for the energy density and the intensity along structure 1:

$$W_1(M) = \rho_s G_1(S, M) + \sigma_A^1 G_1(A, M) + \sigma_B^1 G_1(B, M),$$
$$\mathbf{I}_1(M) = \rho_s \mathbf{H}_1(S, M) + \sigma_A^1 \mathbf{H}_1(A, M) + \sigma_B^1 \mathbf{H}_1(B, M), \tag{4}$$

where G_1 and $\mathbf{H}_1$ come from equation (3). One may clearly identify the contributions of the direct source ρ_s, and the boundary sources σ_A^1 and σ_B^1, in equations (4). For structure 2, equations are similar without the excitation term since structure 2 is not directly excited by a line force,

$$W_2(M) = \sigma_B^2 G_2(B, M) + \sigma_C^2 G_2(C, M),$$
$$\mathbf{I}_2(M) = \sigma_B^2 \mathbf{H}_2(B, M) + \sigma_C^2 \mathbf{H}_2(C, M), \tag{5}$$

and once again, the contributions of each of the boundary sources, σ_B^2 and σ_C^2, are easily recognized.

The acoustical medium description is performed as follows. According to the light fluid hypothesis previously mentioned, structures may be seen as rigid and no diffraction of acoustical waves occurs during their reflection at the surfaces. These phenomena may appear on extremities *A* and *C*, but this assumption allows the use of the specular reflection on baffles as well as on structures. Only structural radiation power sources and their specular reflection are thus to be taken into account in the acoustical energy field description. It should be stressed that what is neglected here is the diffraction of acoustical waves on structural discontinuities, and not the diffraction of the flexural waves. This last process is responsible for the radiation of structures as explained below. For subsonic waves (i.e., below the so-called critical frequency), the radiation of acoustical power is located on structural discontinuities and three kinds of process, occurring at excitation points, structure extremities and junctions of structures, are considered. According to the assumption that propagative waves are uncorrelated, the energy at any point of the

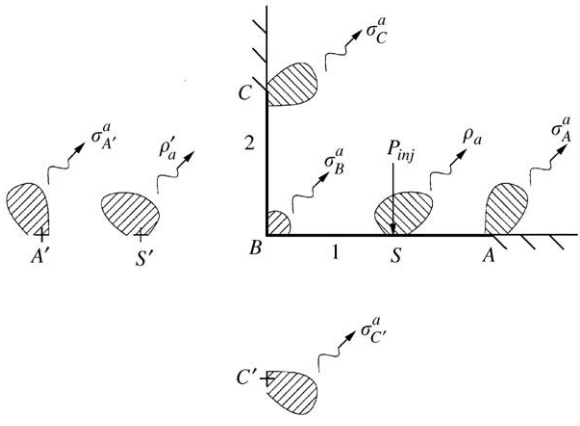

Figure 3. Two baffled, right-angled structures, with the structure 1 being line excited on the point S. Four acoustical sources, σ^a_C, σ^a_B, ρ_a, σ^a_A, and three image sources, σ^a_C, ρ'_a, σ^a_A, are used to describe the acoustical field.

acoustical medium is the sum of the effects of the corresponding acoustical power sources. In addition, assuming the validity of the specular reflection law on the whole boundary of the acoustical medium, the source image method may be used to evaluate the acoustical energy. Seven sources are thus involved in the calculation: ρ_a is located on the excitation line S, σ^a_A and σ^a_C on the extremities A and C, and σ^a_B on the corner B, the first three having their image source on S', A' and C', describing their specular reflection on the opposite face on the acoustical boundary (see Figure 3). The image source ρ'_a is therefore the mirror image of the direct source ρ_a with respect to the reflecting vertical plane containing plate 2: S' is located at the same distance from the plane as S and ρ'_a has the same magnitude as ρ_a with a symmetrically inverted directivity pattern. The source $\sigma^a_{A'}$, is similarly defined with respect to σ^a_A. The source $\sigma^a_{C'}$ is the mirror image of the direct source σ^a_C with respect to the reflecting horizontal plane containing plate 1.

The cylindrical energy solution G_a from equations (3) is used to depict the contribution of all sources. Taking into account the directivity of power sources, the acoustical energy field is obtained as the sum of the contributions of the direct source ρ_a and its image ρ'_a, the corner diffraction source σ^a_B and the extremity diffraction sources σ^a_A and σ^a_C and their images $\sigma^a_{A'}$ and $\sigma^a_{C'}$:

$$W_a(M) = \rho_a(\mathbf{u}_{SM})G_a(S, M) + \rho'_a(\mathbf{u}_{S'M})G_a(S', M) + \sigma^a_A(\mathbf{u}_{AM})G_a(A, M) + \sigma^a_{A'}(\mathbf{u}_{A'M})G_a(A', M)$$

$$+ \sigma^a_B(\mathbf{u}_{BM})G_a(B, M) + \sigma^a_C(\mathbf{u}_{CM})G_a(C, M) + \sigma^a_{C'}(\mathbf{u}_{C'M})G_a(C', M). \quad (6)$$

In order to compute the structural and acoustical energy fields, the source magnitudes ρ and σ of equations (4–6) have to be determined. The first step, detailed in the next section, consists in deriving the corresponding local power balance by solving some canonical problems. The complete system is then solved in section 4.

3. CANONICAL PROBLEMS

In this section, some canonical problems involving the diffraction of subsonic flexural waves into acoustical media are solved in term of power balance. The three diffraction

processes, occurring at excitation points, structure extremities and junctions of structures, are considered.

An identical simplified procedure is used to compute the three canonical problems. The fluid is assumed to be light and the power balance is derived by using the structural *in vacuo* displacement fields. Details of calculations are addressed in Appendix A. In each case, we seek to characterize the relations between the several acoustical and structural intensity terms involved in the energy balance. The corresponding directivities are also determined. Note that the energy flow method may be able to deal with any fluid provided the appropriate canonical problems solutions are used. The solution for any fluid is given for excitation points in reference [10], for baffled structures extremities in reference [11] and for junctions of structures in reference [12].

3.1. EXCITATION POINT

Consider a fluid-loaded infinite plate excited by a line of force or bending moment at a point S. Part of the injected power P_{inj} is supplied to the structure and the other part is diffracted in the acoustical medium with a cylindrical shape. The aim of the canonical calculations is to determine, with consideration for their directivity, the two ratios τ^s_{exci} and τ^a_{exci} of structural power ρ_s and acoustical power ρ_a to the total injected power P_{inj}. Since the structural source ρ_s is shown to be isotropic, its directivity is omitted. The directivity of the acoustical source ρ_a is described by the vector $\mathbf{u}_a$ starting on the excitation line S and describing the acoustical medium.

$$\rho_s = \tau^s_{exci} P_{inj}, \qquad \rho_a(\mathbf{u}_a) = \tau^a_{exci}(\mathbf{u}_a) P_{inj}, \tag{7}$$

where ρ_s and ρ_a are the primary source magnitudes used in equations (4) and (6).

The global power balance implies that the sum of the acoustical and structural powers is equal to the injected power P_{inj}. The structural power is equally shared between both directions of propagation. Thus, it is twice the structural source magnitude ρ_s. To evaluate the acoustical power, the acoustical efficiency τ^a_{exci} must be integrated over a half-cylinder, HC_a, centred on the excitation line. The global power balance, independent of the power being injected, is thus written in terms of both efficiencies,

$$2\tau^s_{exci} + \int_{HC_a} \tau^a_{exci}(\mathbf{u}_a) \mathrm{d}u_a = 1. \tag{8}$$

3.2. STRUCTURE EXTREMITY

A structural wave normally incident on an extremity of a semi-infinite fluid-loaded plate is reflected in the structure and diffracted into the acoustical medium. From the canonical calculation, there are two ratios τ^s_{edge} and τ^a_{edge} of intensities being reflected σ^s and diffracted σ^a over the incident intensity I_{inc}. With $\mathbf{u}_a$ being now the unit vector starting on the edge line and describing the acoustical medium, one obtains

$$\sigma^s = \tau^s_{edge} I_{inc}, \qquad \sigma^a(\mathbf{u}_a) = \tau^a_{edge}(\mathbf{u}_a) I_{inc}. \tag{9}$$

Only one direction, i.e., the reflection direction, is to be taken into account for the structural efficiency τ^s_{edge}. σ^s and σ^a denote the magnitudes of the secondary sources. In the particular

problem of interest, they are located on extremities A and C of structures and are denoted as σ_A^1, σ_C^2 instead of σ^s and σ_A^a, σ_C^a instead of σ^a. These unknowns appear in equations (4–6).

For non-dissipative extremities, the global power balance becomes

$$\tau_{edge}^{s} + \int_{HC_a} \tau_{edge}^{a}(\mathbf{u}_a)\,\mathrm{d}u_a = 1. \tag{10}$$

3.3. JUNCTION OF STRUCTURES

The same phenomena as encountered at the extremities occur at straight junctions of structures. Part of the incident structural power is reflected, another part is transmitted and the last part is diffracted into the acoustical medium. Note that 1 and 2 denote the two plates and $\mathbf{u}_a$ now denotes the unit vector starting on the junction line. The canonical calculation leads to the three power ratios $\tau_{junc}^{i,i}$, $\tau_{junc}^{i,j\neq i}$ and $\tau_{junc}^{i,a}$ of intensities being reflected σ_B^i, transmitted $\sigma_B^{j\neq i}$ and diffracted σ_B^a over the incident intensity I_{inc}^i coming from the plate $i = 1, 2$,

$$\sigma_B^j = \tau_{junc}^{i,j} I_{inc}^i, \qquad \sigma_B^a(\mathbf{u}_a) = \tau_{junc}^{i,a}(\mathbf{u}_a) I_{inc}^i, \quad j = 1, 2. \tag{11}$$

σ_B^j and σ_B^a are the unknown magnitudes of secondary sources located on the junction B, used in equations (4–6).

For non-dissipative junctions, the sum of the total diffracted, reflected and transmitted powers is equal to the incident one:

$$\tau_{junc}^{i,1} + \tau_{junc}^{i,2} + \int_{QC_a} \tau_{junc}^{i,a}(\mathbf{u}_a)\,\mathrm{d}u_a = 1, \tag{12}$$

where the acoustical efficiency $\tau_{junc}^{i,a}$ is now integrated over a quarter of cylinder QC_a corresponding to all directions within the acoustical space delimited by the two right-angled plates.

4. RESOLUTION OF THE SYSTEM

The solution of the vibroacoustic problem is performed by applying the local energy balances (7), (9) and (11) to the whole system using the energy formulations of equations (4–6).

Structures are considered first. Given the injected power P_{inj}, four boundary structural sources σ_A^1, σ_B^1, σ_B^2 and σ_C^2 have to be evaluated. The power balance on the extremity A is written by substituting in the first equation of equation (9) the incident power I_{inc} by the expression $\mathbf{I}_1(A)$ from equations (4). This incident power is shown to be the sum of the intensities coming from both the excitation S and the junction B, projected on the incident direction $\mathbf{u}_1^+$, oriented from B to A. The intensity coming from the excitation S is derived using the first equation of equation (7), and equation (9) becomes

$$\sigma_A^1 = \tau_{edge}^1 [\tau_{exci}^1 P_{inj} \mathbf{H}_1(S, A) + \sigma_B^1 \mathbf{H}_1(B, A)] \cdot \mathbf{u}_1^+. \tag{13}$$

The power balance on the extremity C is similarly derived, with $\mathbf{u}_2^+$ oriented in the direction from B to C,

$$\sigma_C^2 = \tau_{edge}^2[\sigma_B^2 \mathbf{H}_2(B, C)] \cdot \mathbf{u}_2^+ . \tag{14}$$

Finally, the first equation of equation (11) leads to the two energy balances on the junction, by taking into account the incident powers from both structures with reflection and transmission effects,

$$\sigma_B^1 = \tau_{junc}^{1,1}[\tau_{exci}^1 P_{inj} \mathbf{H}_1(S, B) + \sigma_A^1 \mathbf{H}_1(A, B)] \cdot \mathbf{u}_1^- + \tau_{junc}^{2,1}[\sigma_C^2 \mathbf{H}_2(C, B)] \cdot \mathbf{u}_2^- \tag{15}$$

and

$$\sigma_B^2 = \tau_{junc}^{1,2}[\tau_{exci}^1 P_{inj} \mathbf{H}_1(S, B) + \sigma_A^1 \mathbf{H}_1(A, B)] \cdot \mathbf{u}_1^- + \tau_{junc}^{2,2}[\sigma_C^2 \mathbf{H}_2(C, B)] \cdot \mathbf{u}_2^- , \tag{16}$$

where $\mathbf{u}_i^-$ is the opposite to $\mathbf{u}_i^+$. A system of four equations involving the four structural boundary sources is obtained,

$$\mathscr{A} \begin{bmatrix} \sigma_A^1 \\ \sigma_B^1 \\ \sigma_B^2 \\ \sigma_C^2 \end{bmatrix} = P_{inj} \mathscr{B}. \tag{17}$$

The matrix $\mathscr{A}$ and the vector $\mathscr{B}$ are detailed in Appendix B. Substituting the solutions of this system in formulations (4) and (5) leads to the flexural energy densities on both structures.

Acoustical sources are now expressed in terms of structural sources, by applying the appropriate energy balances i.e., the second equation from equation (7) at the excitation point S, the second equation from equation (9) at extremity points A and C, and the second equation from equation (11) at the junction point B:

$$\begin{aligned}
\rho_a &= \tau_{exci}^a P_{inj}, \\
\sigma_A^a &= \tau_{edge}^a[\tau_{exci}^1 P_{inj} \mathbf{H}_1(S, A) + \sigma_B^1 \mathbf{H}_1(B, A)] \cdot \mathbf{u}_1^+, \\
\sigma_C^a &= \tau_{edge}^a[\sigma_B^2 \mathbf{H}_2(B, C)] \cdot \mathbf{u}_2^+, \\
\sigma_B^a &= \tau_{junc}^{1,a}[\tau_{exci}^1 P_{inj} \mathbf{H}_1(S, B) + \sigma_A^1 \mathbf{H}_1(A, B)] \cdot \mathbf{u}_1^- + \tau_{junc}^{2,a}[\sigma_C^2 \mathbf{H}_2(C, B)] \cdot \mathbf{u}_2^- .
\end{aligned} \tag{18}$$

For the sake of clarity, directivities of sources and efficiencies have been omitted. Equation (18) expressed in matrix form is written in terms of the injected power

$$\begin{bmatrix} \rho_a \\ \sigma_A^a \\ \sigma_B^a \\ \sigma_C^a \end{bmatrix} = P_{inj} \mathscr{C}, \tag{19}$$

where the vector $\mathscr{C}$ is detailed in Appendix B. The resultant sources and their corresponding image contributions are introduced in expression (6) to derive the acoustical energy field.

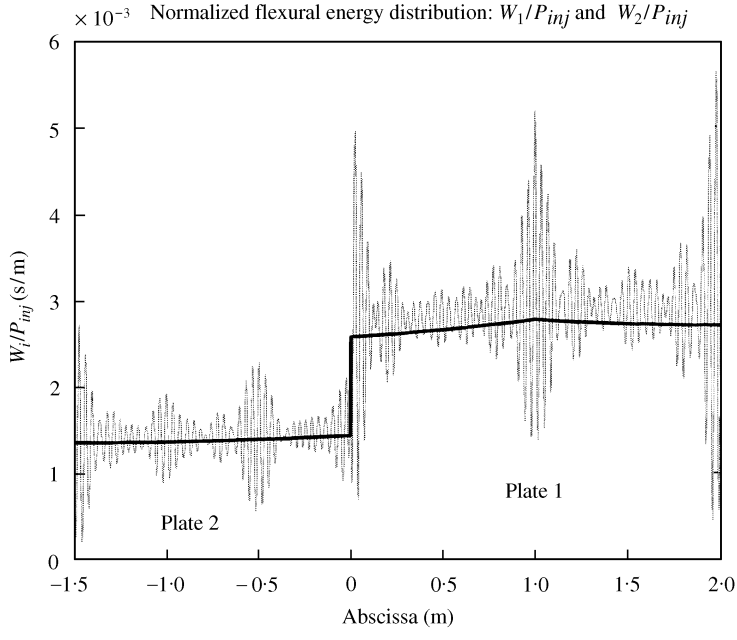

Figure 4. Spatial evolution of the flexural energy normalized by the injected power, on structures 1 and 2 (W_1/P_{inj} and W_2/P_{inj}) at 4000 Hz. Reference results are drawn with grey lines, energy flow approach results with thick lines. The junction of the plates is located on the abscissa $x = 0$ m. The force is applied on the abscissa $x = 1$ m.

5. NUMERICAL RESULTS

Applications have been performed on aluminium plates ($\rho_s = 2800\,\text{kg/m}^3$, $v = 0{\cdot}3$, $E_0 = 7{\cdot}2 \times 10^{10}\,\text{N/m}^2$) coupled with air ($\rho_a = 1{\cdot}3\,\text{kg/m}^3$, $c_a = 340\,\text{m/s}$). The plates are clamped on their extremities, their lengths are $l_1 = 2\,\text{m}$ and $l_2 = 1{\cdot}5\,\text{m}$, and thickness $h = 2 \times 10^{-3}\,\text{m}$. The critical frequency of the system is about 6000 Hz and the simulations are performed at 4000 Hz, below this critical frequency, in order to get subsonic flexural waves. Plate 1 is excited on $x_0 = 1\,\text{m}$, by a line transverse force of unit magnitude. Both plates are damped with coefficients $\eta_1 = \eta_2 = 0{\cdot}5\%$.

Spatial comparisons are carried out. Energy results are compared with reference results averaged over one-third octave band around the central frequency. These reference results are numerical solutions of the equations of motion. They are performed with a boundary integral method using image source kernels to describe the acoustical medium. The energy flow response derives from the resolution of equations (4), (5) and (17) for the structures and equations (6) and (19) for the acoustical medium.

Spatial evolutions of the flexural energy normalized by the injected power, W_1/P_{inj} and W_2/P_{inj} for structures 1 and 2 are drawn in Figure 4. Reference results are in grey lines, energy ones in thick lines. Averaging the reference results over one-third octave band is shown to lead to the smooth pattern of the spatial distribution of the energy in grey. Some strong variations remain, especially near discontinuities ($x = -1{\cdot}5$, 0, 1, 2 m) where the decorrelation of waves does not apply. Except in the vicinity of these points, a good agreement is obtained between the exact and the energy flow methods. Several phenomena explain the pattern of the flexural energy spatial distribution. The global energy level is governed by both the internal damping and the radiation leakages located on

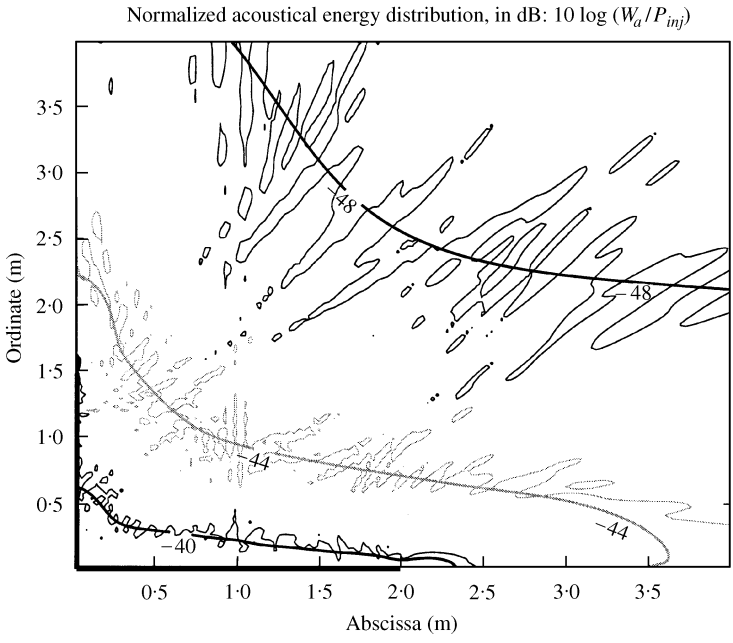

Figure 5. Contour plots of the acoustical energy field normalized by the injected power (expressed in dB: $10\log[W_a/P_{inj}]$), by both reference and energy flow calculations at 4000 Hz. Reference results are drawn with thin lines, energy flow approach results with thick lines. The two assembled plates are drawn in the lower-left corner with bold straight lines.

diffraction points. Note that the internal damping is responsible for the attenuation of the energy during its propagation which explains the slope of the energy level along each structure. The decrease of 3 dB on the junction ($x = 0$ m) is due to transmission effects through the plates junction. These transmission effects prove to be well modelled by the efficiencies $\tau_{junc}^{i,j}$.

Figure 5 shows a map of the acoustical energy normalized by the injected power. Contour plots are drawn in dB ($10\log[W_a/P_{inj}]$) for both calculations. The investigated acoustical domain is square, starting from the corner *B*, and 4 m large. The assembled plates are drawn in the lower-left corner with bold straight lines. Energy approach values are in thick lines. They give a good description of the spatial distribution of the averaged acoustical energy. The modelling of the radiated energy field by a set of diffraction sources proves to be valid at this frequency. Moreover, the assumption that the diffraction sources are uncorrelated is shown to lead to the frequency averaged value of the reference calculation.

Figure 6 shows detailed contributions to the acoustical energy, from the excitation point, extremities and corner diffraction sources, according to the energy flow method. Results are normalized by the injected power and are given in dB ($10\log[W_a/P_{inj}]$). These graphics give an idea of the directivities of each power diffraction source. These directivities are quite smooth when the frequency is low, and become more singular as the frequency approaches the critical frequency. Over the critical frequency, a second radiation process corresponding to the supersonic *leaky* flexural waves is encountered [13]. The resultant radiated waves give rise to interferences with the previously studied diffracted fields in areas called boundary layers [8], and the pressure is no longer described in terms of elementary waves. Thus, the energy flow method, as does the Geometrical Theory of Diffraction, becomes inappropriate in these areas.

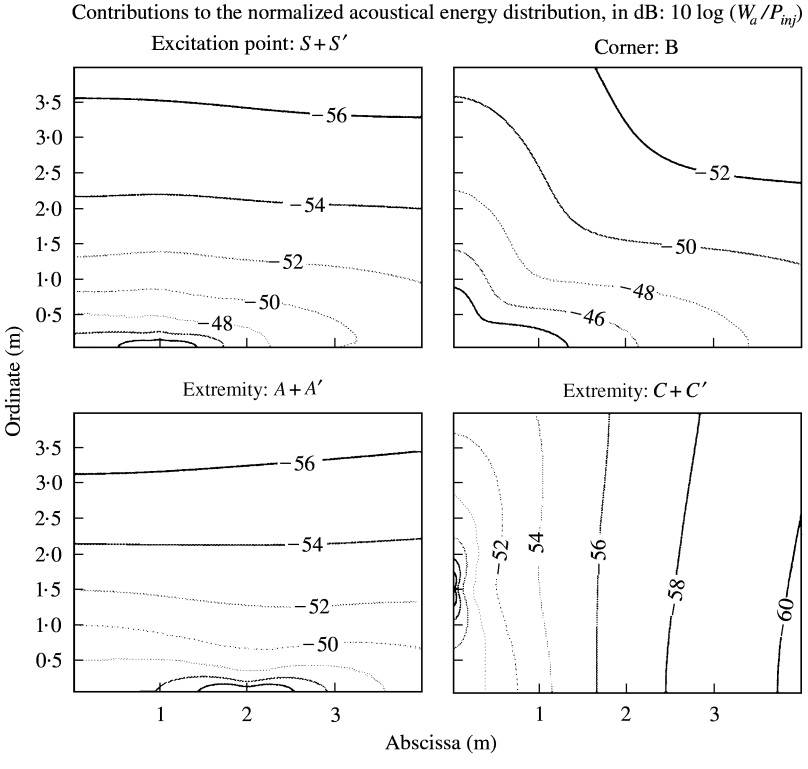

Figure 6. Contour plots of the detailed contributions to the acoustical energy field, from the excitation point, extremities and corner diffraction sources, according to the energy flow method at 4000 Hz. Energies are normalized by the injected power and given in dB: $10\log[W_a/P_{inj}]$.

6. CONCLUSION

The presented energy approach is restricted to the middle- and high-frequency range where the use of the decorrelation assumption and the locality principle is valid. However, in contrast to SEA, it enables the spatial distribution of energy to be predicted when vibration fields are not diffuse, as it is in the case of exterior radiation problems. Compared to the previous energy flows methods, the present development takes into account diffraction effects by adding boundary diffraction power sources to the classical optical ones.

This paper is limited to a two-dimensional system essentially to simplify the solving of the equations of motion necessary for the reference calculation. However, it should be emphasized that canonical problems involved in this example enable the radiation of any structure composed of assembled plates to be calculated.

ACKNOWLEDGMENTS

The authors gratefully acknowledge P. Nicot and E. Garrigues from Dassault-Aviation, France, for their scientific, technical and financial support.

REFERENCES

1. R. H. LYON and R. G. DEJONG 1995 *Theory and Applications of Statistical Energy Analysis.* U.S.A.: Butterworth-Heinemann.

2. O. M. BOUTHIER and R. J. BERNHARD 1995 *Journal of Sound and Vibration* **182**, 149–164. Simple models of the energetics of transversely vibrating plates.
3. A. LE BOT 1998 *Journal of Sound and Vibration* **211**, 537–554. A vibroacoustic model for high frequency analysis.
4. F. BITSIE and R. J. BERNHARD 1997 *Proceedings of Noise and Vibration Conference. Society of Automotive Engineers*. Structure-borne noise prediction using an energy finite element method.
5. F. BITSIE and R. J. BERNHARD 1998 *Noise Control Engineering Journal* **46**. Sensitivity calculations for structural–acoustic EFEM predictions.
6. A. LE BOT and A. BOCQUILLET 2000 *Journal of the Acoustical Society of America* **108**, 1732–1740. Comparison of an integral equation on energy and the ray-tracing technique in room acoustics.
7. J. B. KELLER 1962 *Journal of the Optical Society of America* **52**, 116–130. Geometrical theory of diffraction.
8. D. BOUCHE, F. D. MOLINET and R. MITTRA 1997 *Asymptotic methods in Electromagnetics*. Berlin: Springer-Verlag.
9. V. COTONI, A. LE BOT and L. JEZEQUEL 2000 *Proceedings of International Noise, Nice*. High frequency plate radiation by power flow analysis with experimental validation.
10. P. RANGANATH NAYAK 1971 *Journal of the Acoustical Society of America* **47**, 191–201. Line admittance of infinite isotropic fluid-loaded plates.
11. H. G. DAVIES 1974 *Journal of the Acoustical Society of America* **55**, 213–219. Natural motion of a fluid-loaded semi-infinite membrane.
12. A. N. NORRIS and A. V. OSIPOV 1997 *Journal of the Acoustical Society of America* **101**, 867–876. Structural and acoustical wave interaction at wedge-shaped junction of fluid-loaded plates.
13. A. D. STUART 1976 *Journal of the Acoustical Society of America* **59**, 1170–1174. Acoustic radiation from submerged plates. I. Influence of leaky wave poles.
14. L. CREMER and M. HECKL 1985 *Structure-Borne Sound*. Berlin: Springer-Verlag.
15. G. D. MALYUZHINETS 1955 *Soviet Physical Acoustic* **114**. Radiation of sound from vibrating faces of an arbitrary wedge. Part II.

APPENDIX A: CALCULATION OF SOME CANONICAL PROBLEMS

The simplified calculation of efficiencies (7), (9) and (11) is now summarized. Since the application example corresponds to a two-dimensional problem, the normal incidence is the only one to be considered here. For all cases, the *in vacuo* displacement field is used to compute the radiated acoustical pressure and to derive the resulting power balance. This approach holds only for light fluid loading.

A line-excited fluid-loaded infinite plate, a normally incident flexural wave on a baffled extremity of a fluid-loaded semi-infinite plate, and a normally incident flexural wave on a linear junction of two-fluid-loaded semi-infinite plates are the three canonical problems studied here. All *in vacuo* calculations are performed using a wave decomposition of the structural fields, with both propagative and evanescent terms. By applying the boundary conditions (i.e., efforts equilibrium and displacements continuity), the magnitudes of the several structural waves are determined. They correspond to classical resolutions and they are not detailed here (see reference [14] for example). Starting with the expression of the structural flows carried by the propagative terms, the *in vacuo* power balance is derived.

For the line-excited infinite plate, the same power, equal to half the injected power $P_{inj}/2$, travels in each direction from the excitation. For the flexural wave incident on an extremity of a semi-infinite plate, the energy reflection coefficient is derived as the ratio of the power carried by the reflected wave to the power carried by the incident one. This coefficient is equal to 1 in the case of non-dissipative extremities. Finally, for the junction of two semi-infinite plates, the energy reflection and transmission coefficients noted R_i and T_i are derived as the ratios of the power carried by the reflected wave and the power carried by the transmitted wave to the power carried by the incident wave. In general, their value depends on the incident plate i, and their sum is equal to 1 for non-dissipative junctions.

The fluid is now introduced. For all cases, the same approach may be used to determine the acoustical radiated power. It is presented here for the most general case of two faces with a given displacement field and coupled at an arbitrary angle. The baffled extremity case corresponds to a null displacement field on one face, and a coupling angle equal to π. The line-excited plate corresponds to an angle equal to π with the previously determined displacement field on each face. The Malyuzhinets functions η_{Φ}^{*} [15] are used to determine the acoustical pressure for a wedge of angle 2Φ. Any wave on one face may be written in the form e^{-jkr}, with k complex and r being the radial co-ordinate. Note α which is verifying $\cos\alpha = k/k_a$, where k_a is the acoustical wavenumber. The diffracted pressure is expressed as the Sommerfeld integral [15]

$$p_{\alpha}(r,\theta) = \frac{\rho_a c_a \omega}{2\pi}\left[\int_{-\pi-j\infty}^{-\pi+j\infty} + \int_{\pi-j\infty}^{\pi+j\infty}\right]\eta_{\Phi}^{*}(z+\theta+\Phi,\alpha)e^{-jk_a r\cos z}\,dz, \tag{A.1}$$

where ρ_a and c_a are the density and sound velocity in the fluid. Using the functional properties of η_{Φ}^{*}, and applying the stationary phase method to evaluate the integral, the far-field pressure is written

$$p_{\alpha}(r,\theta) = \frac{\rho_a c_a \omega \sin(\pi/2\Phi)(\pi-\alpha)}{4\Phi\sin(\pi-\alpha)}\frac{1}{[\cos(\pi/2\Phi)(\pi-\alpha)-\sin(\pi/2\Phi)\theta]}\left(\frac{2\pi}{k_a r}\right)^{1/2} e^{j(k_a r+\pi/4)}. \tag{A.2}$$

This calculation is to be applied to each *in vacuo* wave component and the resulting diffracted field $p(r,\theta)$ is obtained by superposition. The corresponding intensity, i.e., the acoustical power radiated into a unity solid angle, is written as $|p(r,\theta)|^2/r\rho_a c_a$. This may be expressed in terms of the incident power in order to complete the local power balance.

Thus for the line excited infinite plate, expressions of the efficiencies (7) are obtained as

$$\tau_{exci}^{a}(\theta) = \frac{|p(r,\theta)|^2}{r\rho_a c_a P_{inj}}, \qquad \tau_{exci}^{s} = 1 - \int_{-\pi/2}^{\pi/2}\tau_{exci}^{a}(\theta)\,d\theta. \tag{A.3}$$

For the extremity diffraction, if I_{inc} is the incident *in vacuo* flexural intensity, efficiencies (9) are written

$$\tau_{edge}^{a}(\theta) = \frac{|p(r,\theta)|^2}{r\rho_a c_a I_{inc}}, \qquad \tau_{edge}^{s} = 1 - \int_{-\pi/2}^{\pi/2}\tau_{edge}^{a}(\theta)\,d\theta. \tag{A.4}$$

The fluid coupling induces structural power losses on the reflection, with an energy reflection coefficient τ_{edge}^{a} less than 1. Finally, for the junction of plates, an assumption must be made to determine the structural efficiencies $\tau_{junc}^{i,i}$ and $\tau_{junc}^{i,j}$ of equation (11). Suppose that the same modification on the *in vacuo* energy coefficients R_i and T_i has to be performed to include the fluid effect, which gives

$$\tau_{junc}^{i,a}(\theta) = \frac{|p(r,\theta)|^2}{r\rho_a c_a I_{inc}}, \qquad \frac{\tau_{junc}^{i,i}}{R_i} = \frac{\tau_{junc}^{i,j}}{T_i} = 1 - \int_{-\Phi}^{\Phi}\tau_{junc}^{a}(\theta)\,d\theta. \tag{A.5}$$

APPENDIX B: POWER BALANCE MATRIX EXPRESSIONS

As in equation (18), the directivities of power sources are omitted in the following expressions for the sake of clarity. Starting with equations (13–16), the matrix $\mathscr{A}$ from equation (17) is shown to be

$$\mathscr{A} = \begin{bmatrix} 1 & -\tau^{1}_{edge}\mathbf{H}_1(B,A)\cdot\mathbf{u}_1^{+} & 0 & 0 \\ -\tau^{1,1}_{junc}\mathbf{H}_1(A,B)\cdot\mathbf{u}_1^{-} & 1 & 0 & -\tau^{2,1}_{junc}\mathbf{H}_2(C,B)\cdot\mathbf{u}_2^{-} \\ -\tau^{1,2}_{junc}\mathbf{H}_1(A,B)\cdot\mathbf{u}_1^{-} & 0 & 1 & -\tau^{2,2}_{junc}\mathbf{H}_2(C,B)\cdot\mathbf{u}_2^{-} \\ 0 & 0 & -\tau^{2}_{edge}\mathbf{H}_2(B,C)\cdot\mathbf{u}_2^{+} & 1 \end{bmatrix}. \tag{B.1}$$

Similarly, the vector $\mathscr{B}$ from equation (17) is

$$\mathscr{B} = \tau^{1}_{exci}\begin{bmatrix} \tau^{1}_{edge}\mathbf{H}_1(S,A)\cdot\mathbf{u}_1^{+} \\ \tau^{1,1}_{junc}\mathbf{H}_1(S,B)\cdot\mathbf{u}_1^{-} \\ \tau^{1,2}_{junc}\mathbf{H}_1(S,B)\cdot\mathbf{u}_1^{-} \\ 0 \end{bmatrix}. \tag{B.2}$$

Expressing equation (18) in matrix form leads to $\mathscr{C} = \mathscr{D} + \mathscr{E}\mathscr{A}^{-1}\mathscr{B}$ with

$$\mathscr{D} = \begin{bmatrix} \tau^{a}_{exci} \\ \tau^{a}_{edge}\tau^{1}_{exci}\mathbf{H}_1(S,A)\cdot\mathbf{u}_1^{+} \\ \tau^{1,a}_{junc}\tau^{1}_{exci}\mathbf{H}_1(S,B)\cdot\mathbf{u}_1^{-} \\ 0 \end{bmatrix}, \tag{B.3}$$

and

$$\mathscr{E} = \begin{bmatrix} 0 & 0 & 0 & 0 \\ 0 & \tau^{a}_{edge}\mathbf{H}_1(B,A)\cdot\mathbf{u}_1^{+} & 0 & 0 \\ \tau^{1,a}_{junc}\mathbf{H}_1(A,B)\cdot\mathbf{u}_1^{-} + & 0 & 0 & \tau^{2,a}_{junc}\mathbf{H}_2(C,B)\cdot\mathbf{u}_2^{-} \\ 0 & 0 & \tau^{a}_{edge}\mathbf{H}_2(B,C)\cdot\mathbf{u}_2^{+} & 0 \end{bmatrix}. \tag{B.4}$$